JCIS Open 3 (2021) 100013

Contents lists available at ScienceDirect

JCIS Open

journal homepage: www.journals.elsevier.com/jcis-open

The search for molecular corks beyond carbon monoxide: A quantum mechanical study of N-Heterocyclic carbene adsorption on Pd/Cu(111) and Pt/Cu(111) single atom alloys

Scott Simpson

Department of Chemistry, St. Bonaventure University, St. Bonaventure, NY, 14778, United States

A B S T R A C T

Periodic Density Functional Theory calculations reveal the potential application of 10 imidazole based N-heterocyclic carbenes (NHCs) to behave as "molecular corks" for hydrogen storage on single atom alloys, comprised of Pd/Cu(111) or Pt/Cu(111). Calculations show that functionalizing the NHC with different electron withdrawing/donating functional groups results in different binding energies of the NHC with the alloy surfaces. The results are compared to DFT calculations of carbon monoxide bound to these alloys. The Huynh electronic parameter is calculated for several simple imidazole NHCs to gauge σ-donor ability, while Se-NMR and P NMR calculations of selenourea derivatives and carbene-phosphinidene adducts, respectively, have been utilized to gauge π-acidity of the NHCs. It is demonstrated that consideration of both σ and π donating/accepting ability must be considered when predicting the surface-adsorbate binding energy. It was found that electron withdrawing groups tend to weaken the NHC-surface interaction while electron donating substituents tend to strengthen the interaction.

1. Introduction

Hydrogen is one of the major alternatives to replace fossil fuels as it has been deemed a clean and renewable energy resource. Hydrogen additionally has the added benefit of having a high energy density with an energy content approximately three times higher than that of gasoline when considering a per weight basis [1–3]. However, before hydrogen usage in transportation, stationary, and portable application can become practically viable hydrogen storage is required to make this dream a reality. Currently a very large liquid or pressurized tank of H_2 gas would be required to be stored on board a vehicle for transportation purposes. Not only is this unpractical for transportation but also is extremely dangerous for numerous reasons. If interstellar travel is ever to become commonplace like it is on different sci-fi television shows (Cowboy Bebop comes to my mind), then a safe, condensed, and high capacity storage device will need to be developed.

To these ends, we propose utilizing a relatively new phenomena, the "molecular corking effect", to solve this conundrum. However, before a device can be built, we must understand how to exert control over every facet of this newly determined effect which has great potential for the storage of hydrogen [4,5]. The screening of potential systems via computations will allow for inexpensive and rapid investigations into targeted systems which show the greatest promise for hydrogen storage. However, due to the relatively recent discovery of this phenomena, there have not been many experimental or theoretical investigations.

The molecular corking effect utilizes single-atom alloys (SAAs). SAAs are metal surfaces that utilize a small amount of catalytically active metals on a relatively inert metal and are known for their exceptional performance, drastic cost reduction, and selectivity [6–8]. Fig. 1 shows a visual example of a Pt/Cu(111) SAA and a schematic representation of the molecular corking effect. The molecular corking effect has been demonstrated by Lucci et al. where small amounts of Pt on a Cu(111) surface is favorable for H_2 activation, spill-over, and release of hydrogen from the surface [9]. They determined that the individual Pt atoms easily dissociate H_2 which then spills over onto the Cu surface as atomistic hydrogen (H). On the Cu surface, atomistic hydrogen is very mobile, only recombines to form H_2 at the Pt sites, and desorbs from the surface at these points as Cu(111) is not capable of dissociating hydrogen gas in ultra high vacuum conditions [10]. This spill-over has also been shown to work for Pd–Au surface alloys as well [11].

The process of the molecular cork effect follows these simple steps: 1) molecular hydrogen (H_2) adsorbs to a Pd/Cu or Pt/Cu alloy; 2) the H_2 bond ruptures due to the interaction of the molecule with the catalytically active metal (Pd or Pt have recently been used) forming atomistic hydrogen (H) on the noble metal (Cu) surface; 3) selective adsorption of ligands to the catalytically active metal prevents the recombination of atomistic hydrogen; 4) temperature is used to dissociate the ligand from the surface, allowing for the recombination of atomistic hydrogen and the liberation of H_2 from the surface. In this mechanism, the surface behaves as the "bottle" while the ligand behaves as the "cork". Recently,

E-mail address: ssimpson@sbu.edu.

https://doi.org/10.1016/j.jciso.2021.100013
Received 8 February 2021; Received in revised form 21 April 2021; Accepted 7 May 2021

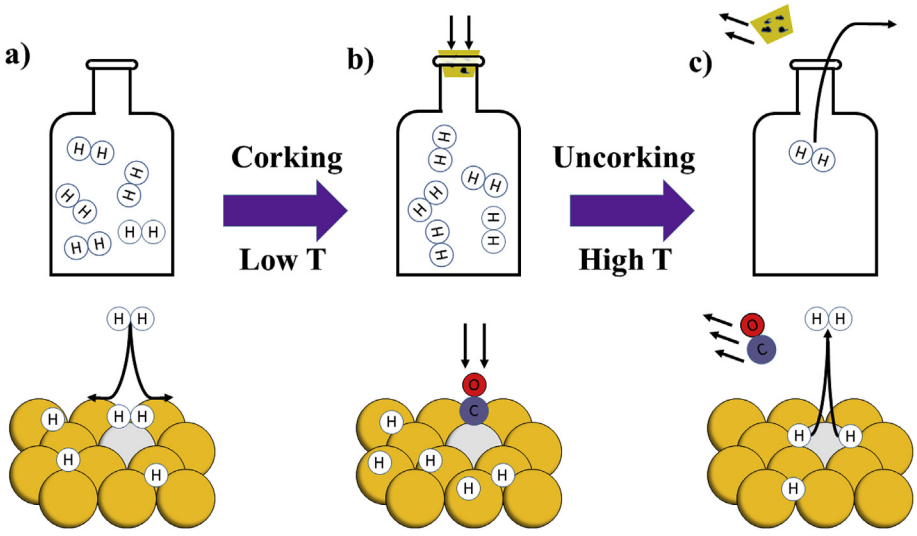

Fig. 1. A schematic representation of the molecular corking effect where the bottle represents the metal surface and the cork represents the ligand carbon monoxide (CO). The top of the figure represents the simplified concept while the bottom represents a more chemical representation. Part (a) show the decomposition of the H_2 molecule and storage phase, part (b) show the corking phase using CO as the cork, and part (c) shows the uncorking phase where the molecular cork leaves allowing the hydrogen to escape from the surface. White/orange/light gray/red/dark gray spheres represent hydrogen/copper/platinum/oxygen/carbon, respectively.

carbon monoxide (CO) was utilized as a cork for a Pd/Cu or a Pt/Cu alloy [4,5]. The previously mentioned study provides evidence that this molecular corking effect does function as CO corks raised the desorption temperature of H_2 from about 210 K to approximately 250 K on Pd/Cu and from 230 K to 280 K on Pt/Cu, respectfully. A schematic representation of this mechanism can be seen in Fig. 1.

It is clear that the temperature at which the hydrogen will leave the metal surface will need to extend above 250 K for practical use. However, it is not just carbon monoxide that can be utilized as a molecular cork. Experiments show that ethyl benzene can also be utilized as a molecular cork on Pd/Cu alloys [4].

Another class of compounds, N-heterocyclic carbenes (NHCs) have been widely used and developed in organometallic chemistry as their σ/π acceptor/donor abilities have been found to be quiet tunable to arrive at a desired molecular geometries [12–14]. ^{77}Se NMR and ^{31}P NMR have been used to gauge the π acceptor abilities of NHCs, while ^{13}C NMR has been used to gauge their σ donating ability and show a path to modulate the electronic structure of these class of compounds [14–17]. In fact, DFT has been used to investigate NHCs on Au, Cu, Ag, and Pt surfaces, showing that NHCs can behave as molecular anchors on these metals [18]. However, there is still minimal studies on NHCs utilize SAAs have be undertaken. A recent studies have shown that derivatization of a NHC can be used to change the binding mode of NHCs on copper and gold surfaces using scanning tunneling microscopy (STM), X-ray photoelectron spectroscopy (XPS), other surface techniques, and DFT [18–21]. In an attempt to replace thiols, NHCs have been shown to be a promising replacement as molecular anchors as use of sensors, microelectronics, surface protectants, and even drug delivery applications on gold surfaces [22–28]. The aforementioned experimental results clearly show that NHCs are excellent molecular anchors for transition-metal surfaces, and therefore would be potentially viable molecular corks. To demonstrate this, we provide preliminary evidence to show that the substituents on the NHCs can be used to modulate the strength of the interaction between surface and adsorbate.

1.1. Computational details

All periodic DFT calculations were conducted using the VASP.5.3.3 software package and the optPBE-vdW functional to account for dispersion forces [29,30]. The projector augmented wave (PAW) method [31,32] was used to treat the core states along with a planewave energy cut-off of 500 eV, and the C/N/O/F 2s/2p, H 1s, S/P 3s/3p, Cu 4s/3d, Pd 5s/4d, and Pt 6s/5d electrons were treated explicitly. The Γ-Centered Monkhorst-Pack scheme was used to generate k-point meshes, and we

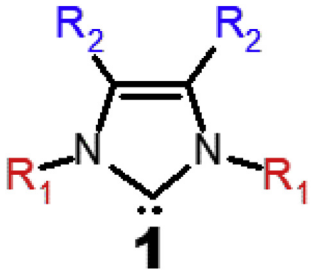

Fig. 2. The N-heterocyclic carbene imidazole backbone considered in this study. R_1 and R_2 have been modified with the different substituents listed in Table 1.

employed a 9 × 9 × 1 K-mesh, which gave rise to energies that were converged to within 1 meV/atom of energies compute with a larger k-mesh. A three-layer 48 atom slab was used to simulate the Cu(111) surface. During geometry optimizations involving the slab, the adsorbate and top layer of the slab were permitted to relax while the bottom two layers of the slab were fixed. In the case of periodic SAA calculations, a single atom of Cu in the surface layer of the slab was replaced by Pd or Pt atom, similar to what is described to Darby at el [5]. A dipole correction was applied along the direction perpendicular to the metal surface using the LDIPOL tag as implemented in VASP. Isolated molecules were optimized in a 15 Å × 15 Å x 15 Å unit cell. To determine the impact of the inclusion of approximate non-local dispersion, the revised PBE functional (revPBE) was used [33]. The results of these calculations are contained in the supporting information (SI).

Molecular calculations were conducted using the TURBOmole software package [34] using the BP86 functional [35,36] and a def2-TZVPD basis [37,38] for each element. Vibrational frequencies were calculated for these optimized geometries to ensure a minimum on the potential energy surface was determined. NMR shielding constant calculations were with the previously described basis functions and functional for all systems other than our Huynh Electronic Parameter (HEP) calculations. In calculations of the HEP, the dhf-TZVP basis for each of the lighter elements and the dhf-ecp was utilized for Pd atoms.

2. Results and discussion

Our initial investigation reported herein utilize the simple NHC with an imidazole backbone, as seen in Fig. 2. We have selected a variety of different substituents that will impact the σ/π donor/acceptor properties

Table 1
Isotropic chemical shielding (σ), diamagnetic shielding component (σ_d) and paramagnetic shielding component (σ_p) of selenourea and carbene-phosphinidene adducts for the NHC imidazole-based molecules calculated using TURBOMOLE, the BP86 density functional, and the def2-TZVPD basis set.

R_1	R_2	Se-σ (ppm)	σ_d (ppm)	σ_p (ppm)	P-σ (ppm)	σ_d (ppm)	σ_p (ppm)
H	H	1696.8	3001.4	−1304.6	289.7	949.0	−659.3
H	F	1651.0	3000.8	−1349.9	282.4	947.7	−665.3
H	Cl	1615.6	3001.0	−1385.4	277.4	948.2	−670.8
H	CH_3	1722.6	3002.1	−1279.5	289.6	947.8	−658.2
CH_3	H	1710.1	3002.1	−1292.0	307.4	947.8	−640.4
H	CF_3	1629.4	3002.3	−1372.9	281.4	947.5	−666.1
H	NH_2	1722.3	3002.0	−1279.2	291.0	947.2	−656.1
H	NO_2	1438.1	3001.3	−1563.3	248.2	947.1	−698.9
H	COH	1609.4	3001.5	−1392.1	289.9	943.5	−653.6
H	$N(CH_3)_2$	1767.7	3002.9	−1235.2	288.0	946.0	−658.0

of the NHCs. We have previously shown that functionalization can impact the surface-adsorbate interface for benzene derivatives on Cu(111) and Ag (111) [39,40]. First, we consider a variety of different NMR techniques that have been shown to quantify the σ/π donor/-acceptor interactions of different NHCs using molecular DFT calculations. Then we quantify the overall interaction of the NHCs with Pd/Cu(111) or Pt/Cu(111) SAAs using periodic optPBE-vdW calculations. Finally, we then compare the energetics of these NHCs to determine plausible higher-temperature molecular corks.

2.1. Gauging π-acidity of the NHCs

It is well known that NHCs not only interact with transition metals via σ-interactions, but also π-interactions. As previously stated, Se-NMR and P NMR have been utilized to gauge π-acidity. To these ends, we have conducted NMR calculations of the selenoureas and carbene-phosphinidene adducts of these NHCs [14]. The results of these calculations can be seen in Table 1.

Our calculations show that the electron withdrawing groups, such as $–CF_3$ or $–NO_2$, lower the overall isotropic chemical shielding. It is apparent that the paramagnetic shielding component (σ_p) decreases the more electron withdrawing the substituent, while the diamagnetic shielding component (σ_d) remains essentially constant. The opposite trend can be said to be true for electron donating groups, such as $–CH_3$, or $–N(CH_3)_2$, which the overall isotropic chemical shielding and σ_p values increase as donor ability increases. Studies have shown that the more upfield/shielded the Se signal of the selenourea, the less π-acidic the NHC [14–17]. The opposite is said to be true; the more downfield these signals, the more π-acidic the NHC. The most π-acidic groups were determined to be $–NO_2$, and –COH while the least acidic were found to be $–NH_2$, $–CH_3$, and $–N(CH_3)_2$.

Generally, the Se-σ trends match the P-σ, with some notable exceptions such as –COH. We attribute this discrepancy to the number of energetically accessible conformers of the carbene-phosphinidene adducts, which can have widely different isotropic P-σ values. While this is not an issue in experiment, our calculations only account for one conformer in our calculations. This could be curbed by taking an average of a weighted Boltzmann distribution of the different conformers. However, we elect to draw trends from the selenoureas as their trends have been shown to experimentally match that of carbene-phosphinidene adducts [17]. Additionally, the Se-carbene bond does not have as much conformational flexibility as the phosphinidene-carbene bonds. However, these NMR signals provide only a gauge of the π-interactions of the NHCs. To gauge the σ-acidity/basicity, one must consider other parameters, such as the Huynh electronic parameter.

2.2. Gauging σ-donor strength of the NHCs

The Huynh electronic parameter (HEP) utilizes ^{13}C NMR spectroscopy to gauge the primarily σ-donor strength of a ligand [14,41,42]. The carbene carbon signal of the $^{i}Pr_2$bimy "reporter" ligand is used as the reporting metric of the HEP. When this signal is shifted more upfield (more shielded), the competing ligand is a weaker donor, while a downfield (less shielded) indicates a stronger donor ligand. HEP has been considered to be more capable of determining subtle variations in the ligand's electronic structure compared to other electronic parameters, such as the Tolman electronic parameter. We have calculated the HEP for the NHCs previously mentioned in this study (Table 2). The NHCs functionalized with $–NO_2$ and $–CF_3$ are the weakest σ-donor ligands while $–N(CH_3)_2$, $–NH_2$, and $–CH_3$ functionalized NHCs were found to be the strongest σ-donor ligands.

Table 2
The HEP isotropic C chemical shift (HEP) as calculated using TURBOMOLE, the BP86 density functional, and the dhf-TZVP basis set. TMS was used as a reference standard with the same computational methodology.

R_1	R_2	HEP (ppm)
H	H	196.5
H	F	194.7
H	Cl	194.8
H	CH_3	197.4
CH_3	H	198.4
H	CF_3	193.8
H	NH_2	197.6
H	NO_2	191.7
H	COH	193.3
H	$N(CH_3)_2$	196.9

2.3. Periodic calculations

Using periodic optPBE-vdW calculations, we have conducted geometry optimizations for the interaction of these NHC interacting with a SAA Pd/Cu(111) and Pt/Cu(111) alloys at a surface coverage of 0.01442 molecules/$Å^2$. First, one must probe the potential energy surface of this surface-adsorbate system to gauge the potential of these adsorbate molecules prowess as molecular corks. Does the NHC even prefer to bind to the catalytical active metal? Without this binding site preference, the adsorbate molecule would not be useable as a molecular cork. To confirm this, we conduct a series of calculations where the NHC is optimized at different positions on the metal surface. In one calculation, the NHC interacts with one of the copper atoms in the surface layer whereas the NHC interacts with the Pd/Pt atom in the other calculation. The results of these calculations are tabulated in Table 3. We have determined all of the tested NHCs favor binding to the catalytically active metals, rather than a copper surface atom by approximately 5/11 kcal/mol for Pd/Cu(111) and Pt/Cu(111), respectively. The lowest energy geometries of the NHC-alloy interactions were found to adopt a geometry with the plane of the NHC molecule perpendicular to the plane of the surface rather than parallel to the surface plane, similar to Fig. 3. Bakker et al. have shown that less sterically substituted NHCs adopt a similar binding mode on Au (111) using scanning tunneling microscopy (STM), X-ray photoelectron spectroscopy (XPS), and DFT calculations [20].

Table 3
The carbene carbon-Pd/Pt bond length (C–Pd Dist), the differences in energy between the NHC binding via Pd/Pt vs. a copper surface atom (E_{diff}), the binding energy (BE), and overall Bader charges of the adsorbed NHC (q_{NHC}) for differently substituted NHCs using optPBE-vdW. Energies are reported in kcal/mol. The carbene carbon to Pd/Pt atom is also reported in angstroms. Charges are reported in e (elementary charge).

R_1		Pd/Cu(111) SAA				Pt/Cu(111) SAA			
	R_2	C–Pd Dist (Å)	E_{diff} (kcal/mol)	BE (kcal/mol)	q_{NHC} (e)	C–Pt Dist (Å)	E_{diff} (kcal/mol)	BE (kcal/mol)	q_{NHC} (e)
H	H	2.0612	5.0	−43.0	+0.011	2.0176	11.6	−49.5	−0.011
H	F	2.0500	4.1	−40.2	−0.041	2.0121	10.0	−46.4	−0.057
H	Cl	2.0452	4.1	−41.6	−0.102	2.0061	10.0	−47.9	−0.105
H	CH_3	2.0592	4.3	−46.3	−0.008	2.0194	10.1	−52.9	+0.028
CH_3	H	2.1175	6.0	−39.8	−0.205	2.0518	11.4	−45.4	−0.217
H	CF_3	2.0530	5.9	−40.7	−0.127	2.0082	11.7	−47.1	−0.113
H	COH	2.0473	5.0	−31.3	−0.119	2.0027	11.8	−37.9	−0.102
H	NH_2	2.0493	3.5	−46.5	+0.010	2.0161	9.5	−53.0	−0.031
H	NO_2	2.0579	10.9	−40.7	−0.222	2.0109	11.5	−47.1	−0.264
H	$N(CH_3)_2$	2.0472	4.3	−49.3	+0.007	2.0124	11.4	−56.1	−0.049

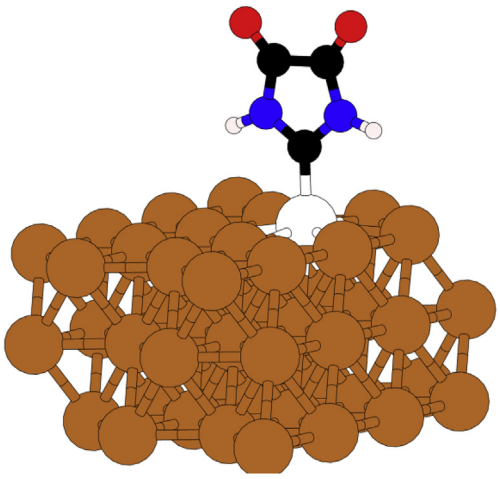

Fig. 3. The optimized simulation cell of an NHC (R_1 = H, R_2 = O) on Pd/Cu(111). Hydrogen, carbon, nitrogen, oxygen, copper, and palladium atoms are colored white, black, blue, red, orange, and silver, respectively.

Next, the strength of the surface-adsorbate interaction, the binding energy, must be considered to rule out unsuitable corks. The binding energy (BE) was calculated using the following formula:

$$BE = E_{surf\text{-}ads} - E_{surf} - E_{ads}$$

Where $E_{surf\text{-}ads}$ is the energy of the SAA surface interacting with the NHC adsorbate, E_{surf} is the energy of the isolated SAA surface, and E_{abs} is the energy of the isolated NHC molecule. Therefore, a negative energy show an energetically favorable interaction. Generally, the NHCs have a higher binding energy on the Pt–Cu SAA compared to the Pd–Cu SAA. The average bond length of the NHC-metal bond is longer on Pd/Cu(111) in comparison to Pt/Cu(111).

Considering the influence of the substituents, the more electron withdrawing groups, such as R_2 = -NO_2, –COH, –CF_3, have a weaker BE compared to the unfunctionalized NHC while electron donating groups, such as R_2 = -$N(CH_3)_2$,-CH_3, –NH_2, have a stronger binding energy for both alloys. Some general trends can be established based upon our previously mentioned isotropic Se shielding and HEP values:

1. The more π-acidic the NHC, and therefore the lower Se isotropic shielding, the weaker the binding energy compared to the unfunctionalized imidazole.
2. The lower the HEP value, the weaker the surface-adsorbate interaction.

To determine the flow of charge between the surface and the adsorbate, Bader charges were computed for each system [43]. Generally, NHCs bound to the Pt/Cu(111) experienced a large magnitude of charge transfer than those on Pd/Cu(111) for a given functionalization. In the majority of the cases, the NHC acquired a surplus amount of charge while the surface lost charge. The exceptions were for the NHCs substituted with R_1 = -H/R_2 = -H, –NH_2, –$N(CH_3)_2$ on Pd/Cu(111) and only R_1 = -H/R_2 = -CH_3 for Pt/Cu(111).

Table 4
The binding energy (BE) for differently surface coverages of NHCs on Pd/Cu(111) and Pt/Cu(111) using optPBE-vdW, reported in kcal/mol.

Coverage (molecules/Å^2)	Pd/Cu(111) SAA		Pt/Cu(111) SAA	
	BE (kcal/mol)	C–Pd Dist (Å)	BE (kcal/mol)	C–Pt Dist (Å)
$8.653 \cdot 10^{-3}$	−44.1	2.0549	−50.9	2.0163
$1.082 \cdot 10^{-2}$	−44.1	2.0561	−50.7	2.0178
$1.442 \cdot 10^{-2}$	−43.0	2.0612	−49.5	2.0176
$2.163 \cdot 10^{-2}$	−42.8	2.0468	−49.3	2.0129

However, another factor that will dictate the NHC-surface interaction beyond modulation of the electronic structure is steric hindrance. This is clearly illustrated when comparing the interaction of the NHC that has been substituted with –CH_3/-H and –H/-CH_3, R_1/R_2 respectively. The binding energy of –CH_3/-H is greater than that of the –H/-CH_3 substituted NHC by approximately 7 kcal/mol, yet the calculated shielding of the two NHCs, contained in Table 1, indicate that these molecules have similar π-acidity. Additionally, the C–Pd lengths and the C–Pt lengths are significantly longer for the –CH_3/-H NHC compared to the –H/-CH_3. Excluding the sterically hindered case of –H/-CH_3, it is clear to see that the strength of the NHC-surface interaction can be modulated via the substituents on the NHC as the binding energies range of approximately 20 kcal/mol of the tested adsorbates.

It is also important to know that coverage of adsorbate molecules on the surface can influence the surface-adsorbate interaction [44]. To these ends we have optimized the simplest of our previously mentioned NHCs (R_1 = R_2 = -H) with varying surface coverages to demonstrate the impact of coverage on the binding energy (Table 4). We also make note that the surface coverage of Pt/Pd atoms matches the coverage of molecules, as only one of these atoms is included in the simulation cell. Unsurprisingly, as the surface coverage increases the binding energy of the NHC to the alloy surface decreases for both Pd/Cu(111) and Pt/Cu(111). This is attributed to charge redistribution upon molecular adsorption and the intermolecular attraction between adjacent adsorbate molecules [44–48]. As seen for both alloys, increasing the molecular coverage decreases the magnitude of the binding energy by approximately 4 kcal/mol for the coverages considered herein. This demonstrates that surface coverage needs to be considered when considering a ligand's potential to behave as a molecular cork.

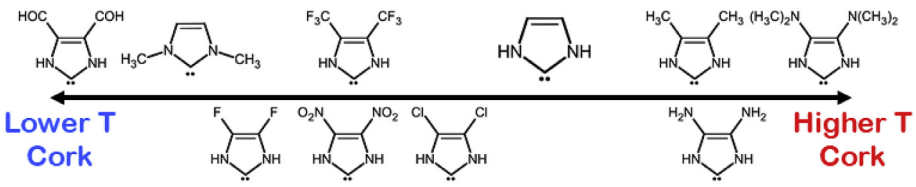

Fig. 4. Approximate scale of molecular cork ability of N-heterocyclic carbene adsorbates on Pd/Cu(111) and on Pt/Cu(111).

2.4. Categorizing the plausible molecular corks

We have also calculated the binding energy of carbon monoxide (CO) on both alloys. Similar to the study by Darby et al. [5,49], we found that the most favorable binding site of CO on Pt/Cu(111) was on the Pt top site. We conclude that the same binding site trend for Pd/Cu(111), with the CO bound to a top site above the Pd, is the most energetically preferable by approximately 15 kcal/mol. They also determined that the binding energy of CO to Pt/Cu(111) was −27.4 kcal/mol using periodic RPBE calculations [5]. For Pd/Cu(111), the RPBE binding energy of CO was calculated to be 19.4 kcal/mol [49]. Another manuscript by Illas et al. utilized a cluster model to study the interaction of CO on a Pd_1Cu_{12} cluster [50]. They found that the binding energy was 17.3 kcal/mol using the hybrid B3LYP functional, and a near negligible binding energy of 0.7 kcal/mol using Hartree-Fock (HF) theory. This highlights the importance of including correlation to accurately model these surface-adsorbate systems. Using optPBE-vdW, we calculate the binding energy of CO to these alloys to be −30.8 kcal/mol for Pt/Cu(111) and −24.2 kcal/mol for Pd/Cu(111) at a coverage of 0.01442 molecules/$Å^2$, respectively. A Bader charge analysis shows that the CO adsorbate molecule accumulates 0.103e on Pd/Cu(111) and 0.270e on Pt/Cu(111). Our traditional GGA revPBE calculations, which did not include non-local correlation, at coverage of 0.01075 molecules/$Å^2$, show a weaker binding energy for each SAA. The binding energy was calculated to be −19.4 kcal/mol for Pd/Cu(111) and −27.2 kcal/mol for Pt/Cu(111). A Bader charge analysis shows that the CO adsorbate molecule accumulates 0.188e on Pd/Cu(111) and 0.211e on Pt/Cu(111). This shows the inclusion of dispersion forces in surface-adsorbate systems is required.

The Polanyi-Wigner equation indicates that systems with a higher binding energy will have a higher desorption temperature, assuming other parameters such as coverage and frequency factor, remain constant.[51] Therefore, based upon binding energies of the NHCs to the alloy surfaces, we have split the NHCs listed in Table 3 into higher/lower temperature molecular corks. In all cases the NHCs should desorb at a temperature higher than CO on both alloys. A summary of the results can be seen in Fig. 4. The lowest temperature cork is predicted to be the NHC(R_1 = -COH, R_2 = -H) while NHC(R_1 = -H, R_2 = -$N(CH_3)_2$) is predicted to be the highest temperature cork for both Pd/Cu(111) and Pt/Cu(111). However, a useful cork will have a desorption temperature that is fitting for its application. Therefore, we plan to pursue a way to predict the desorption temperature of these NHCs using computations in the future.

3. Conclusions

In summary, we have predicted the capacity of several imidazole-based NHCs to behave as molecular corks for hydrogen storage applications on Pd/Cu(111) and Pt/Cu(111) alloys using periodic DFT-vdW calculations. Calculations show that functionalizing the NHC with different electron withdrawing/donating functional groups results in different binding energies of the NHC with the alloy surfaces. The surface coverage was also shown to impact the binding energy of simple NHC to the alloys. HEP and Se-NMR calculations were calculated and used to rationalize binding trends. Therefore, both σ and π donating/accepting ability must be considered when predicting the surface-adsorbate binding energy. Finally, functionalization for the imidazole-based NHC can modulated the desired application/desorption temperature.

Declaration of competing interest

The authors declare that they have no known competing financial interests or personal relationships that could have appeared to influence the work reported in this paper.

Acknowledgements

The author acknowledge National Science Foundation (Award #1904825) for support of this research, and the Donors of the American Chemical Society Petroleum Research Fund (PRF-58954-UNI5). The author also acknowledge Professor Kellie Gast for providing useful comments. Any opinions, findings, conclusions, or recommendations expressed in this publication are those of the author and do not necessarily reflect the view of the NSF.

Appendix A. Supplementary data

Supplementary data to this article can be found online at https://doi.org/10.1016/j.jciso.2021.100013.

References

[1] M.P. Suh, H.J. Park, T.K. Prasadm, D.W. Lim, Hydrogen storage in metal-organic frameworks, Chem. Rev. 122 (2012) 782–835.
[2] W. Grochala, E.P. Edwards, Thermal decomposition of non-interstitial hydrides for the storage and production of hydrogen, Chem. Rev. 104 (2004) 1283–1315.
[3] M. Hirscher, V.A. Yartys, M. Baricco, J.B. von Colbe, D. Blanchard, R.C. Bowman, D.P. Broom, C.E. Buckley, F. Chang, P. Chen, et al., Materials for hydrogen-based energy storage – past, recent progress and future outlook, J. Alloys Compd. 827 (2020) 153548.
[4] M.D. Marcinkowski, A.D. Jewell, M. Stamatakis, M.B. Boucher, E.A. Lewis, C.J. Murphy, G. Kyriakou, E.C.H. Sykes, Controlling a spillover pathway with the molecular cork effect, Nat. Mater. 12 (2013) 523–528.
[5] M.T. Darby, F.R. Lucci, M.D. Marcinkowski, A.J. Therrien, A. Michaelides, M. Stamatakis, E.C.H. Sykes, Carbon monoxide mediated hydrogen release from PtCu single-atom alloys: the punctured molecular cork effect, J. Phys. Chem. C 123 (2019) 10419–10428.
[6] R.T. Hannagan, G. Giannakakis, M. Flytzani-Stephanopoulos, C.H. Sykes, Single-atom alloy catalysis, Chem. Rev. 230 (2020) 12044–12088.
[7] N. Niancai Cheng, L. Lei Zhang, K. Kieran Doyle-Davis, X. Sun, Single-atom catalysts: from design to application, Electrochem. En. Rev. 2 (2019) 539–573.
[8] G. Kyriakou, M.B. Boucher, A.D. Jewell, E.A. Lewis, T.J. Lawton, A.E. Baber, H.L. Tierney, M. Flytzani-Stephanopoulos, E.C.H. Sykes, Isolated metal atom geometries as a strategy for selective heterogeneous hydrogenations, Science 335 (2012) 1209–1212.
[9] F. Lucci, M. Marcinkowski, T. Lawton, E.C.H. Sykes, H_2 activation and spillover on catalytically relevant Pt-Cu single atom alloys, J. Phys. Chem. C 119 (2015) 24351–24357.
[10] G. Anger, A. Winkler, K. Rendulic, Adsorption and desorption kinetics in the systems H_2/Cu(111), H_2/Cu(110) and H_2/Cu(100), Surf. Sci. 220 (1989) 1–17.
[11] F.R. Lucci, M.T. Darby, M.F.G. Mattera, C.J. Ivimey, A.J. Therrien, A. Michaelides, M. Stamatakis, E.C.H. Sykes, Controlling hydrogen activation, spillover, and desorption with Pd−Au single-atom alloys, J. Phys. Chem. Lett. 7 (2016) 480–485.
[12] A.A. Grineva, O.A. Filippov, S.E. Nefedov, N. Lugan, V. César, D.A. Valyaev, Direct access to IMesF and IMesF2 by electrophilic fluorination of abnormal N-heterocyclic carbenes, Organometallics 38 (2019) 2330–2337.
[13] J.C. Bernhammer, G. Frison, H.V. Huynh, Electronic structure trends in N-heterocyclic carbenes (NHCs) with varying number of nitrogen atoms and NHC-Transition-Metal bond properties, Chem. Eur J. 19 (2013) 12892–12905.
[14] H.V. Huynh, Electronic properties of N-heterocyclic carbenes and their experimental determination, Chem. Rev. 118 (2018) 9457–9492.

[15] O. Back, M. Henry-Ellinger, C.D. Martin, D. Martin, G. Bertrand, ^{31}PNMR chemical shifts of carbene–phosphinidene adducts as an indicator of the π-accepting properties of carbenes, Angew. Chem. Int. Ed. 52 (2013) 2939–2943.
[16] L. Falivene, L. Cavallo, Theoretical NMR spectroscopy of N-heterocyclic carbenes and their metal complexes, Coord. Chem. Rev. 344 (2017) 101–114.
[17] S.V.C. Vummaleti, D.J. Nelson, A. Poater, A. Gómez-Suárez, D.B. Cordes, A.M.Z. Slawin, S.P. Nolan, L. Cavallo, What can NMR spectroscopy of selenoureas and phosphinidenes teach us about the p-accepting abilities of N-heterocyclic carbenes? Chem. Sci. 6 (2015) 1895–1904.
[18] K. Chang, J.G. Chen, Q. Lu, M.J. Cheng, Grand canonical quantum mechanical study of the effect of the electrode potential on N-heterocyclic carbene adsorption on Au surfaces, J. Phys. Chem. C 121 (2017) 24618–24625.
[19] C.R. Larrea, C.J. Baddeley, M.R. Narouz, N.J. Mosey, J.H. Horton, C.M. Crudden, N-Heterocyclic carbene self-assembled monolayers on copper and gold: dramatic effect of wingtip groups on binding, orientation and assembly, ChemPhysChem 18 (2017) 3536.
[20] A. Bakker, A. Timmer, E. Kolodzeiski, M. Freitag, H.Y. Gao, H. Mönig, S. Amirjalayer, F. Glorius, H. Fuchs, Elucidating the binding modes of N-heterocyclic carbenes on a gold surface, J. Am. Chem. Soc. 140 (2018) 11889–11892.
[21] K. Chang, J.G. Chen, Q. Lu, M.J. Cheng, Quantum mechanical study of N-heterocyclic carbene adsorption on Au surfaces, J. Phys. Chem. 121 (2017) 2674–2682.
[22] A.V. Zhukhovitskiy, M.J. MacLeod, J.A. Johnson, Carbene ligands in surface chemistry: from stabilization of discrete elemental allotropes to modification of nanoscale and bulk substrates, Chem. Rev. 115 (2015) 11503–11532.
[23] T. Weidner, J.E. Baio, A. Mundstock, C. Grosse, S. Karthauser, C. Bruhn, U. Siemeling, NHC-based self-assembled monolayers on solid gold substrates, Aust. J. Chem. 64 (2011) 1177–1179.
[24] A.V. Zhukhovitskiy, M.G. Mavros, T. Van Voorhis, J.A. Johnson, Addressable carbene anchors for gold surfaces, J. Am. Chem. Soc. 135 (2013) 7418–7421.
[25] C.M. Crudden, J.H. Horton, Ebralidze II, O.V. Zenkina, A.B. McLean, B. Drevniok, Z. She, H.B. Kraatz, N.J. Mosey, T. Seki, et al., Ultra stable self-assembled monolayers of N-heterocyclic carbenes on gold, Nat. Chem. 6 (2014) 409–414.
[26] C.M. Crudden, J.H. Horton, M.R. Narouz, Z. Li, C.A. Smith, K. Munro, C.J. Baddeley, C.R. Larrea, B. Drevniok, B. Thanabalasingam, et al., Simple direct formation of self-assembled N-heterocyclic carbene monolayers on gold and their application in biosensing, Nat. Commun. 7 (2016) 12654.
[27] G. Wang, A. Ruhling, S. Amirjalayer, M. Knor, J.B. Ernst, C. Richter, H.J. Gao, A. Timmer, H.Y. Gao, N.L. Doltsinis, et al., Ballbot-type motion of N-heterocyclic carbenes on gold surfaces, Nat. Chem. 9 (2016) 152–156.
[28] S. Engel, E.C. Fritz, B.J. Ravoo, New trends in the functionalization of metallic gold: from organosulfur ligands to N-heterocyclic carbenes, Chem. Soc. Rev. 46 (2017) 2057–2075.
[29] J. Klimeš, D.R. Bowler, A. Michaelides, Van der Waals density functionals applied to solids, Phys. Rev. B 83 (2011) 195131.
[30] J. Klimeš, D.R. Bowler, A. Michaelides, Chemical accuracy for the van der Waals density functional, J. Phys.-Condens. Mat. 22 (2009), 022201.
[31] P. Blöchl, Projector augmented-wave method, Phys. Rev. B Condens. Matter 50 (1994) 17953.
[32] G. Kresse, D. Joubert, From ultrasoft pseudopotentials to the projector augmented-wave method, Phys. Rev. B 59 (1999) 1758.
[33] J.P. Perdew, K. Burke, M. Ernzerhof, Generalized gradient approximation made simple, Phys. Rev. Lett. 77 (1996) 3865–3868.
[34] TURBOmole v7.3.
[35] J.P. Perdew, Density-functional approximation for the correlation energy of the inhomogeneous electron gas, Phys. Rev. B 33 (1986) 8822–8824.
[36] A.D. Becke, Density-functional exchange-energy approximation with correct asymptotic behaviour, Phys. Rev. 38 (1988) 3098–3100.
[37] D. Rappoport, F. Furche, Property-optimized Gaussian basis sets for molecular response calculations, J. Chem. Phys. 133 (2010) 134105.
[38] F. Welgend, R. Ahlrichs, Balanced basis sets of split valence, triple zeta valence and quadruple zeta valence quality for H to Rn: design and assessment of accuracy, Phys. Chem. Chem. Phys. 7 (2005) 3297–3305.
[39] S. Simpson, E. Zurek, Substituted benzene derivatives on the Cu(111) surface, J. Phys. Chem. C 116 (2012) 12636–12643.
[40] D.P. Miller, S. Simpson, N. Tyminska, E. Zurek, Benzene derivatives adsorbed to the Ag(111) surface: binding sites and electronic structure, J. Chem. Phys. 142 (2015) 101924.
[41] Q. Teng, H.V. Huynh, A unified ligand electronic parameter based on ^{13}C NMR spectroscopy of N-heterocyclic carbene complexes, Dalton Trans. 46 (2017) 614–627.
[42] H.V. Huynh, Y. Han, R. Jothibasu, J.A. Tang, ^{13}C NMR spectroscopic determination of ligand donor strengths using N-heterocyclic carbene complexes of palladium 9II0, Organometallics 28 (2009) 5395–5404.
[43] W. Tang, E. Sanville, G. Henkelman, A grid-based bader analysis algorithm without lattice bias, J. Phys. Condens. Matter 21 (2009), 084204.
[44] S. Simpson, D.A. Kunkel, J. Hooper, J. Nitz, P.A. Dowben, L. Routaboul, P. Braunstein, B. Doudin, A. Enders, E. Zurek, Coverage-dependent interactions at the organics-metal interface: quinonoid zwitterions on au(111), J. Phys. Chem. C 117 (2013) 16406–16415.
[45] P.S. Bagus, V. Staemmler, C. Wöll, Exchangelike effects for closed-shell adsorbates: interface dipole and work function, Phys. Rev. Lett. 89 (2002) 1–4, 096104.
[46] A.D. Jewell, S.M. Simpson, A. Enders, E. Zurek, E.C.H. Sykes, Magic electret clusters of 4-fluorostyrene on metal surfaces, J. Phys. Chem. Lett. 3 (2012) 2069–2075.
[47] G. Rojas, S. Simpson, X. Chen, D.A. Kunkel, J. Nitz, J. Xiao, P.A. Dowben, E. Zurek, A. Enders, Surface state engineering of Molecule−Molecule interactions, Phys. Chem. Chem. Phys. 14 (2012) 4971–4976.
[48] J. Colin, C.J. Murphy, D.P. Miller, S. Simpson, A. Baggett, A. Pronschinske, M.L. Liriano, A.J. Therrien, A. Enders, S.-Y. Liu, E. Zurek, et al., Charge transfer induced magic cluster formation of azaborine heterocycles on noble metal surfaces, *J. Phys. Chem. C.* 120 (2016) 6020–6030.
[49] M.T. Darby, E.C.H. Sykes, A. Michaelides, M. Stamatakis, Carbon monoxide poisoning resistance and structural stability of single atom alloys, Top. Catal. 61 (2018) 428–438.
[50] F. Illas, N. López, J.M. Ricart, A. Clotet, J.C. Conesa, M. Fernández-Garcia, Interaction of CO and NO with PdCu(111), J. Phys. Chem. B 102 (1998) 8017–8023.
[51] C.J. Murphy, A. Baggett, D.P. Miller, S. Simpson, M.D. Marcinkowski, M.F.G. Mattera, A. Pronschinske, A. Therrien, M.L. Liriano, E. Zurek, et al., Effect of BN/CC isosterism on thermodynamics of surface and bulk binding; 1,2-dihydro-1,2-azaborine vs. benzene, J. Phys. Chem. C 17 (2015) 12265–12272.